11th ANKARA INTERNATIONAL AEROSPACE CONFERENCE **AIAC-2021-167**
8-10 September 2021 - METU, Ankara TURKEY

COMPUTATIONAL INVESTIGATION OF AERODYNAMIC AND AEROELASTIC BEHAVIOR OF AN ICED AIRFOIL

Esra SAYDAN[1], Emine YURDUSAY[2]
University of Samsun
Samsun, Turkiye

Kemal GUNDOGAN[3]
Istanbul Technical University
Istanbul, Turkiye

Ahmet Selim DURNA[4]
University of Samsun
Samsun, Turkiye

ABSTRACT

Building an icing model on the blade for calculating steady loads and the structural response to the loads gives different behavior which can affect the aerodynamic efficiency, natural frequencies, deflections, reduced lifetime and it should be calculated with the real outputs of the system. The loads can be able to calculate and determine on icing models and constructed on design assumptions to prove the blade fatigue life and survival for its desired life. Our concern is the accumulation of ice on the blades can affect the performance due to aerodynamic efficiency and on the other hand, because of the increase of ice mass loads, the life of the components can decrease. In this study, the 2D symmetrical NACA 0012 and the NACA 64-618 airfoils used in wind turbines are preferred. The numerical simulations are performed by ANSYS Fluent using two different grid topologies for the clean NACA 0012 airfoil and two different turbulence models Spalart-Allmaras and k-ω for NACA 64-618. The effects of icing on drag and lift coefficient are obtained through simulations. These data are compared with experimental ones obtained by special wind tunnels such as IRT. The results are consistent with the experimental data in the literature. Apart from the CFD investigation, modeling of the system aero-elastically becomes very important due to the dynamic response of the blade construction. It can change angle of attack instantly and cause performance reduction and make the system unstable due to vibration. Aeroelastic responses of the blade were obtained by coupling those aerodynamic and structural models. The present model was also validated with the results of the other aeroelastic simulations. The aim of this side of the study is to use the validated numerical model to assess the effects of extreme wind speed conditions and blade fatigue life. To accomplish this side of the study, aeroelastic analysis is performed with an in-house tool considering blade coordinates and boundary conditions. Damping and modal analysis results are compared for drag and lift coefficients with different angles of attack in clean and iced airfoils. It can be seen those obtaining results show there is a misalignment and frequency differences between normal and glazed iced blade model. It is shown that glazed iced blade should investigate aerodynamic efficiency with aeroelastic effect under different wind speed conditions.

[1] Undergraduate student in Aerospace Engineering Department, Email: 16960083@samsun.edu.tr
[2] Undergraduate student in Aerospace Engineering Department, Email: 16960026@samsun.edu.tr
[3] Ph.D. student in Aerospace Engineering Department, Email: gundogank@itu.edu.tr
[4] Asst. Prof. in Aerospace Engineering Department, Email: ahmetselim.durna@samsun.edu.tr

INTRODUCTION

Most of aircraft crashes or wind turbine failures occur in bad weather conditions. Often, this is due to the icing on the blade. The icing that occurs on the system surfaces is caused by supercooled droplets. Water can exist as a liquid at a temperature below 0°C, this state is called supercooling. As soon as the cloud droplets touch the surface, they can freeze and form rime ice, or the stream can flow down the surface and then freeze to form a glazed ice structure. Ice accumulation on the control surfaces, wings and flight data sensors affects both the performance and operational safety of the system. For this reason, evaluating the performance degradation due to icing has become very important in the design and certification stages [Anderson, 2004].

Liquid water content (LWC), water droplet diameter (MVD) and ambient temperature are the main factors in icing. The liquid water content is the measure of the mass of the liquid water in a cloud in a specified volume of dry air. Ambient temperature affects the type of ice formed on the system when it is exposed to liquid water droplets. Droplet median volume diameter (MVD) is also an important factor affecting the icing process. The most usual icing is formed by cloud water droplets of size smaller than 50 microns MVD. When MVD is higher than 50 microns the clouds contain supercooled water droplets [Alzaili, 2012]. There are two different types of ice related to icing: Glaze Ice and Rime Ice. Rime ice occurs when air temperatures are lower than freezing temperatures and is opaque. In this type of ice, droplets tend to freeze when in contact with the solid surface. Glaze (horn) ice, on the other hand, is known for its translucent structure and occurs when air temperatures are close to freezing. Mixed ice is a mixture of glaze ice and rime ice [Brown, 2013].

According to the study conducted by Richard Hann [Hann, 2018] on the NREL S826 airfoil in 2018, rime ice forms consistently, but this is not the case for mixed and glazed ice. Yet all types of ice adversely affect aerodynamic performance by reducing maximum lift, reducing stall angle, and increasing friction. Addy [Addy, 2000] conducted an experimental study in 2000. According to this study, the aerodynamic effects of icing were investigated according to 3 different airfoil types. This study experimentally expressed the performance loss that was tried to be revealed by CFD analysis. [Homola, Virk, Wallenius, Nicklasson, & Sundsbø, 2010] have used a two-steps method, combining TURBICE and ANSYS Fluent to investigate the effect of ice similarly on a NACA 64-618 profile. They found that the lift coefficient was reduced in all cases and the smallest change was observed in the case of rime ice. During the CFD simulations, it was found that the horn type glaze ice shape causes the largest separation, which leads to a significantly reduced lift and higher drag coefficient. [Etemaddar, Hansen, & Moan, 2013] has also used the same profile in their numerical analysis. In their study, they combined LEWICE code with ANSYS Fluent and pointed out that the ice load increases with liquid water content (LWC), median volumetric diameter (MVD) and relative wind speed.

Apart from the CFD investigation, modeling of the system aero-elastically becomes very important due to the dynamic response of the blade construction. It can change angle of attack instantly and cause performance reduction and make the system unstable due to vibration. Aeroelastic responses of the blade were obtained by coupling those aerodynamic and structural models. The present model was also validated with the results of the other aeroelastic simulations. The aim of this side of the study is to use the validated numerical model to assess the effects of extreme wind speed conditions and blade fatigue life. In aeroelastic side of the study, it is also obtained relatively accurate results within this margin based on BEM theory. Related loads are obtained with blade operational modes and conditions. In order to perform aeroelastic analysis, both aerodynamic and structural model must be quite reliable. From the literature, it can be seen those previous aeroelastic calculations used simple methods for aerodynamic and structural model such as blade element momentum method (BEM) as mentioned by Glauert [Glauert, 1935]. The aerodynamic model is modelled to handle dynamic characteristics and effects from large deflection. BEM Theory is used to solve these equations and Finite element method (FEM) is used with Timoshenko-beam elements for structural modeling.

Blade deformation alters angle of attack, which causes edgewise vibration. Structural vibration velocity alters relative wind speed, which causes flapwise vibration by external wind conditions. Blade is investigated under these circumstances and load simulations are performed with a linear BEM model assumed with loads applied to undeformed structure and displacement are linear. There are several papers on the Blade Element Momentum (BEM) theory to model the induced wind speeds due to the aerodynamic forces mentioned above. Pirrung et al. [Pirrung, 2017] has also shown that BEM based aeroelastic models under predict the stability limit by 5-10% compared to a more comprehensive near wake model.

The aim of the study is to investigate the aerodynamic and aeroelastic effects of icing on NACA 64-618 airfoil at angles of attack (α) between 0º and 12º. The numerical results will be compared with the experimental study in the literature. Damping and modal analysis results will be compared for drag and lift coefficients with different angles of attack in clean and iced airfoils. Blade characteristics and behaviour will be shown between normal and glazed iced blade model.

METHOD

Geometry

The geometry data for NACA 64-618 obtained from reference [Etemaddar et al., 2013] are used for validation in this part of the study.

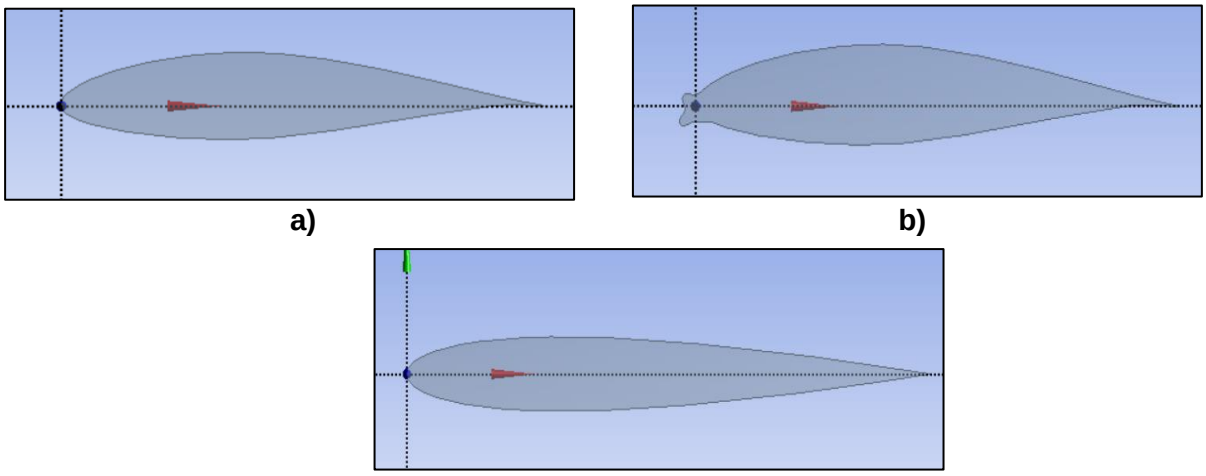

Figure 1: Geometry: a) Clean NACA 64-618 b) Iced NACA 64-618 c) Clean NACA 0012 Built in Design Modeler.

Mesh Structure

This paper also includes a comparative study of two different mesh topologies, the structured and the unstructured mesh built around NACA0012. The numerical results are validated against experimental data collected by Abbott and Doenhoff (1959). Figure 2 shows structured (right) and unstructured (left) grids built around the airfoil. A C-type mesh with the computational area grid extending from 20 chord upstream to 30 chords downstream from the 1m chord profile. The unstructured mesh consisted 985043 cells while the structured consisted a total of 1455860 cells. Both mesh had the maximum skewness around 0.5. A total of 20 inflation layers with the first layer height set to 1x $\mathbf{10^{-5}}$were added to the mesh to obtain y+ value around 1. Both cases were simulated using the k-ω SST turbulence model with the intermittency transition model. Consequently, the numerical results were validated against experimental data collected by Abbott and Doenhoff (1959)

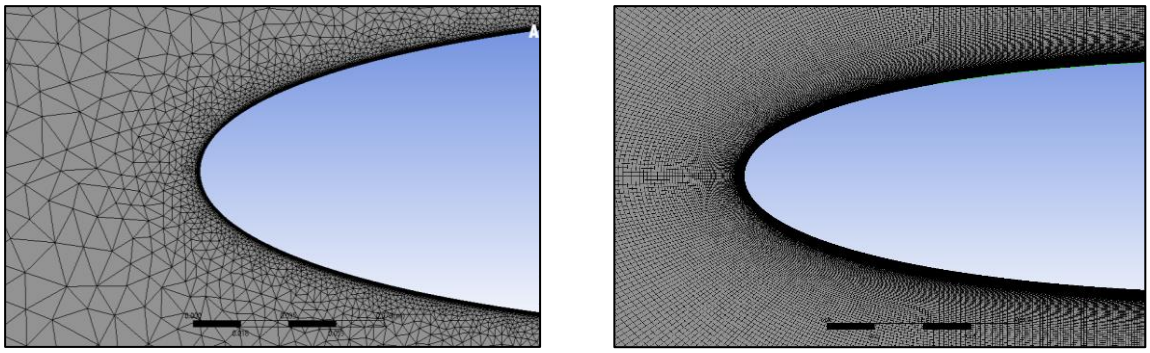

a) **b)**

Figure 1: Mesh Topologies Built Around NACA 0012 a) Unstructured b) Structured

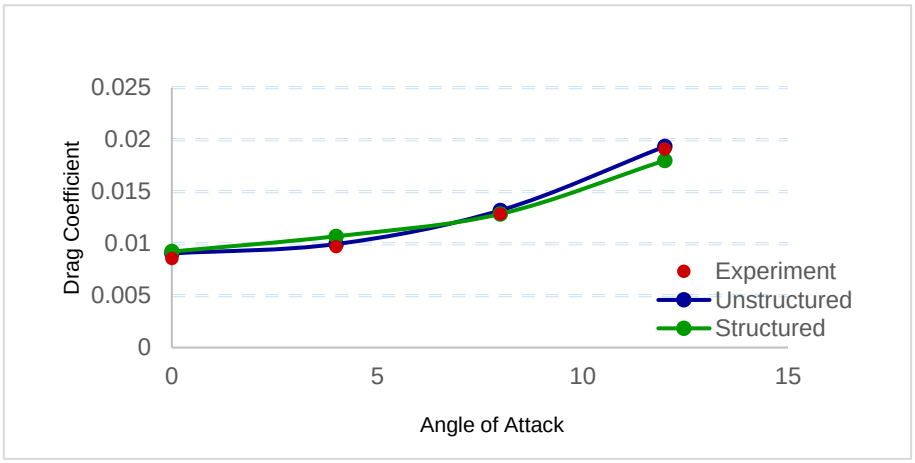

a)

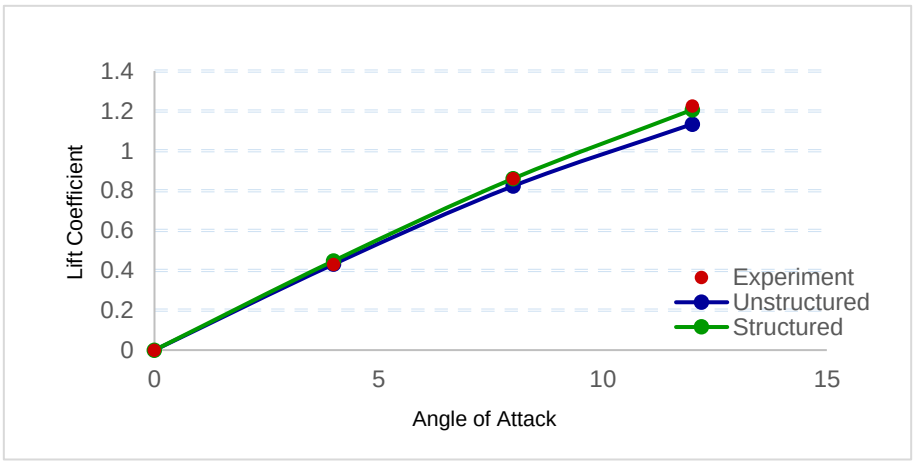

b)

Figure 2: Comparison of Experimental and Numerical Results with Structured and Unstructured Grids for Clean NACA0012 Airfoil. a) Drag coefficient b) Lift coefficient

It is seen from Figure 3 both structured and unstructured grids show good agreement with experimental data. The creation of structured mesh in case of glaze ice will be extremely difficult and time consuming; additionally, because the mesh structure forces a fine resolution in areas where it is not required, the distribution of cells may be less efficient in structured mesh. As a result, the computational time necessary to generate a structured mesh is elevated and may result in an unnecessarily high cell count. On the contrary, triangular meshes generally require less setup time and allow more freedom in the placement of cells, thus

allowing clustering of elements in specified regions of the flow domain. Thus, the simulations will be carried out using unstructured grid topology.

Mesh Independency Study

A mesh independence study was performed for clean NACA 64-618 airfoil by the mesh being continually refined until the solutions could be termed “grid independent”. The calculated results, lift and drag coefficients were studied at angles of attack α=0º, 4º, 8º and 12º with coarse, medium and fine grids. These grids have a total of 498093, 996187 and 1992374 cell numbers, respectively. There was a negligible difference between the results and thus, in order to select an optimal grid size to save computation time, the medium grid consisting of 996187 cells was used in this study. In Figure 4, drag and lift coefficients for three grids are shown.

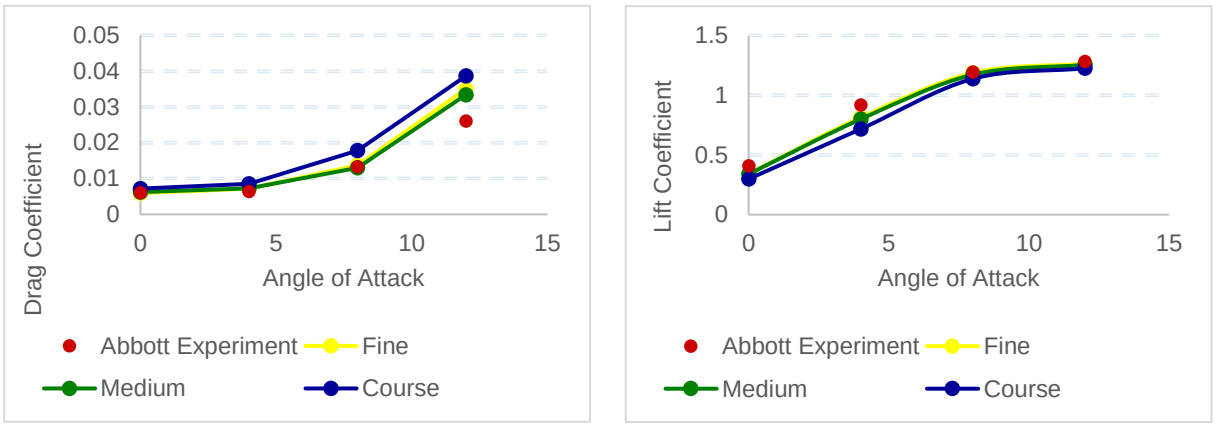

a) **b)**

Figure 4: Mesh independency Study a) Drag coefficient b) Lift coefficient

Mesh Generation

A C-shaped computational domain was chosen because of the ease with which it allows for uniform distribution of cells in the far field and was built in the ANSYS Meshing. The overall size of the domain was defined in number of chords before and after the airfoil. The radius of the C-part was set 30 and the length of the rectangle was set as 20 times the chords. The domain had to be large enough so that the flow at the boundaries was not altered by the airfoil. A more accurate flow solution is obtained from high number of elements; at the expense of computational time, but to set the cells enlarging from the airfoil is a clustering strategy which can significantly reduce the number of cells without deteriorating the accuracy of the flow solutions. In order to achieve this goal, it was decided to create dense grids near the surface and downstream of the airfoil only. Moreover, characteristics and calculation of the flow near the airfoil are crucial, the grid as generated considers a distance to the first element close enough to the airfoil to allow the turbulence model to resolve the viscous sublayer. A total of 20 inflation layers with the first layer height set to $1x10^{-5}$ were added to the mesh to obtain the y+ value around 1 as the validity of turbulence models depends on the dimensionless distance y+ from the wall to the center of the first element. To avoid high skewed elements near the wall the element size around the airfoil was set at 0.001 mm. Maximum skewness was set up to 0.6 to generate high quality mesh. These approaches led to a mesh with approximately 996187 cells for the clean airfoil case and 1034929 for the iced airfoil case.

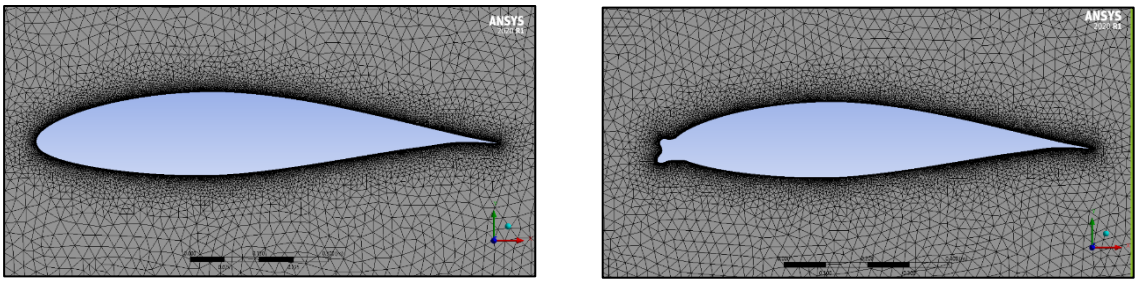

a) b)

Figure 5: Grids around a) Clean NACA 64-618 Airfoil b) Glaze Iced NACA 64-618 Airfoil.

Numerical Modeling

A finite volume-based solver CFD tool ANSYS Fluent is used to perform the analysis. During simulations, some procedures or approaches have been followed in order to increase the accuracy and decrease the computation time needed for each individual simulation. For this study, an incompressible, steady and unsteady RANS model is applied. The clean was simulated using k-ω SST turbulence model and the iced airfoil was simulated using two different turbulence models, the one-equation Spalart-Allmaras and the two-equation k-ω SST turbulence model. For k-ω SST turbulence model the transition effects were characterized by intermittency transition model. The convergence criteria for the residuals were set to 10^{-5} and the SIMPLE algorithm with second-order upwind scheme were adopted. The density and the dynamic viscosity for all cases were kept as 1.225 and 1.7894 respectively. The angles of attack simulated are 0º, 4º, 8º and 12º. For transient simulations, the time-step size was chosen in such a way that the maximum Courant–Freidrichs-Lewy number in the simulation was 0.1. The numeric results are validated against experimental data. The validation is carried out by considering the input and boundary conditions shown in Table 1.

Table 1: Inputs and Boundary Conditions for Numerical Modeling

	NACA 0012	NACA 64618	
	Clean	Clean	Iced
Reynold Number	$3x10^6$	$3x10^6$	$2x10^6$
Velocity (m/s.)	43.822	43.822	50
Reference Length (m.)	1	1	0.6044

Aeroelastic Modeling

For a given model setup**,** a blade substructure coordinate system is defined for each blade according to one of three definitions. The system is fixed to the hub with origin**.** The difference between the coordinate system definitions is the position of the origin identified**.** The blade changes its angle of attack under the wind conditions, but the blade is also affected by the dynamic effect of the structure. The blade characteristics will be shown with eigenmodes linearly. These effects are shown by performing aeroelastic modal analysis about an isotropic deflected steady state model. Wind speed can be defined to produce the modal parameters including aerodynamic equations in analysis and unsteady effect of trailing edge separation. For load simulations, damping and modal analysis are performed with blade coordinates and boundary conditions defined in Figure 6. There are some defined normal and iced blade positions which beam element data is written in defined model.

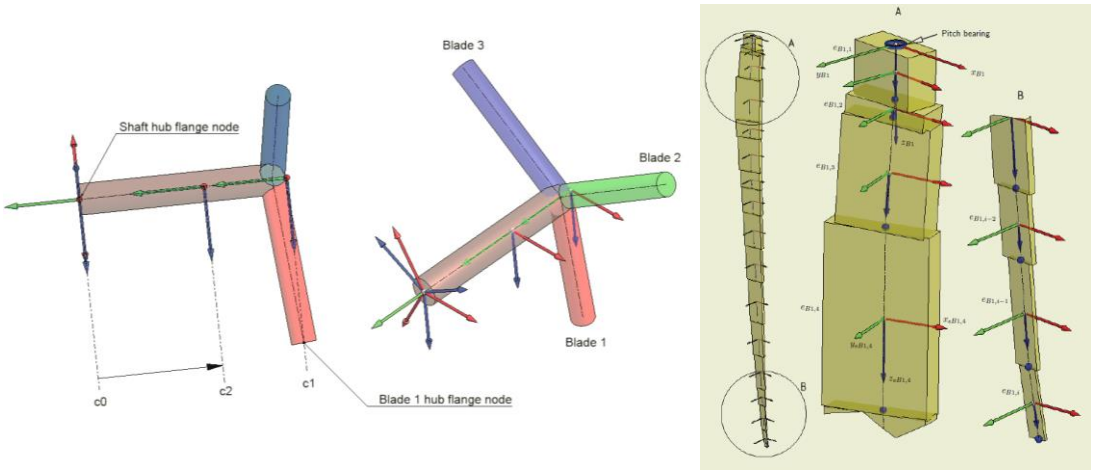

(a) **(b)**

Figure 6: a) Fixed Blade-Rotor Coordinate Systems b) Blade Beam Element Coordinate Systems

The blade coordinate system is fixed to the blade root identified as the center. The z axis is perpendicular to the flange and directed towards the blade tip. The x axis is directed towards the leading edge of the blade. With zero blade angle, the x and y axis are parallel with the corresponding axes of the blade design coordinate system. The x axis is directed towards the leading edge of the blade. Initially, the geometry is defined for the blade with zero flap and edge angles. This geometry corresponds to the design geometry as represented in the blade. The x and y-coordinates are usually read from blade geometry common with aerodynamic model. Finally, the structural pitch angle defines the orientation of the element coordinate system and the design geometry is defined. Turbulence intensity values in Figure 7, obtained from International Standard: IEC 61400-1 2005 Ed3 for the normal turbulence model (NTM) and extreme turbulence model (ETM) are used between 3 m/s and 25 m/s wind conditions.

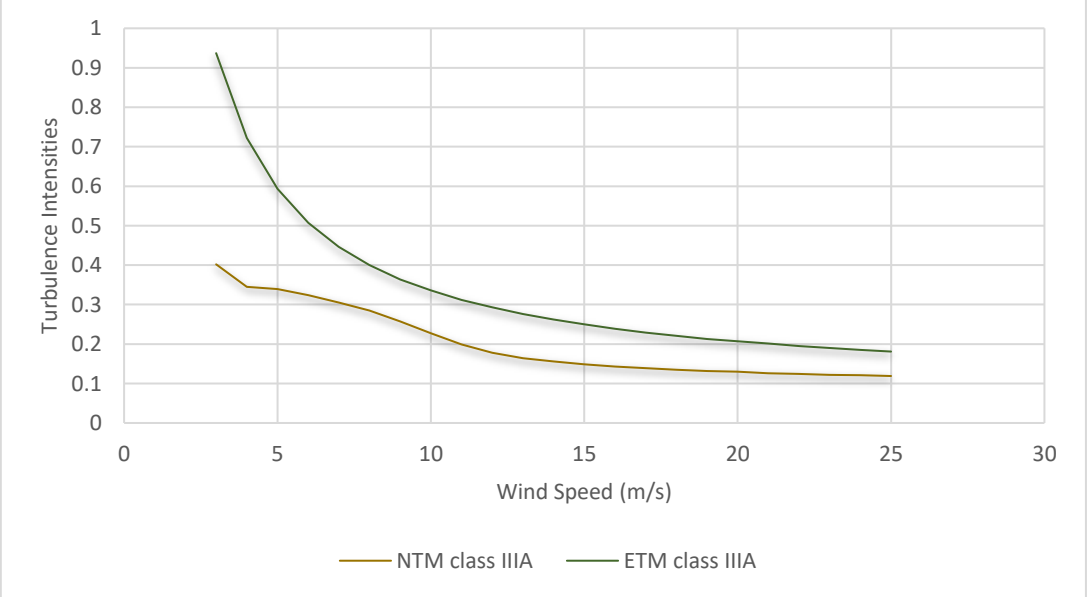

Figure 7: Standard Turbulence Intensity Values for NTM and ETM (IEC 61400-1, 2005)

It is possible to define the damping at a blade using modal based damping. This allows to specify the damping for each mode individually. In comparison, when using the Rayleigh damping approach, one could only define a single flap, edge, and torsion blade modes and the

single fore-aft, side-side, and torsion tower modes without introducing unwanted rigid body damping. The results will be indicated the mode number and associated percent logarithmic decrement value. The damping of unspecified high order modes is automatically allocated the damping value of the last user defined logarithmic decrement modal damping value. Degree of freedom can be literally defined as Figure 8 and flapwise bending moment (FBM), edgewise bending moment (EBM) and torsion effect can be modeled and can be shown along the blade chord.

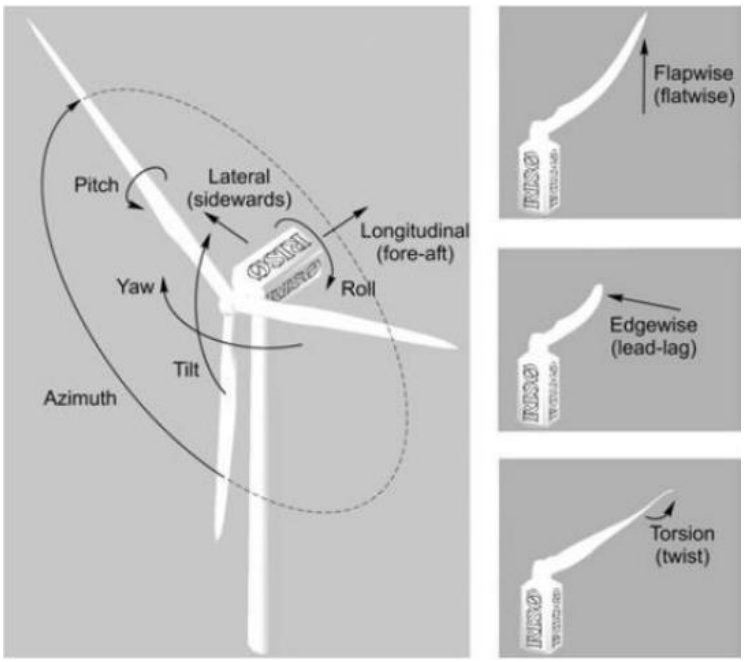

Figure 8: Flapwise, Edgewise and Torsion degree of freedom terminology (Hansen, 2007)

The blade is expressed with all degrees of freedom vector $\boldsymbol{u}=[\boldsymbol{u}_b T \ \boldsymbol{u}_i T]T$. The vector components represent the boundary degrees of freedom and the internal degrees of freedom. The split in degrees of freedom between the vectors defines the type of boundary conditions. In the case where damping is to be defined for a free-free structure, the vector $\boldsymbol{u}b$ will be empty. For a clamped structure the vector $\boldsymbol{u}b$ will contain three orthogonal displacement degrees of freedom and three orthogonal rotation degrees of freedom.

Following the Craig-Bampton (1968) super element formulation, one can relate the internal degrees of freedom to the generalized degrees of freedom of the fixed base system. We can finally write the dynamic equation of motion (including damping) using the Craig-Bampton transform expressed as:

$$\boldsymbol{\lambda} = \begin{bmatrix} 2\omega_1\zeta_1 & \cdots & 0 \\ \vdots & \ddots & \vdots \\ 0 & \cdots & 2\omega_i\zeta_i \end{bmatrix}$$

where $2\,\omega_i\,\zeta_i$ is modal damping, $\omega_i\,\zeta_i$ is the undamped angular frequencies associated with the mode shapes contained in the matrix. The critical damping ratio ζ_i is defined with the associated logarithmic decrement which enables to control damping of each mode of the blade.

The reference node can be identified by counting from the blade tip using negative integers. The blade is modeled using 17 nodes so, the blade tip node is identified using a total of 16 nodes using a negative integer. Using eigenvalue analysis, an equivalent full inertia of the blades is added to the blade substructure. The position of the blade is also defined by yaw, azimuth and pitch angles when calculating the inertia. The calculated natural frequencies will

change slightly depending on the prescribed values as this changes the center of gravity of the rigid blade. These inertia properties are also modeled in the mass property file.

Table 1: Inputs and Boundary Conditions for Load Analysis

Parameters	**Value**
Air density [kg/m3]	1.136
Shear [alpha]	0.224
Inflow angle [°]	0
Lateral turbulence ratio s2/s1	0.7
Vertical turbulence ratio s3/s1	0.5
Weibull scale factor (A-factor)	10
Weibull shape factor (k-factor)	4
Average velocity [m/s]	11.2
Extreme wind velocity (10 min average) [m/s] for clean airfoil	42.5
Extreme wind velocity (3 sec average) [m/s] for clean airfoil	59.5
Extreme wind velocity (10 min average) [m/s] for iced airfoil	50
Extreme wind velocity (3 sec average) [m/s] for iced airfoil	70
Blade substructure tip node	16
Design standard	IEC_Ed3

RESULTS

Clean Airfoil

The contours of static pressure and velocity magnitude obtained from α=0º, 4º, 8º and 12º from CFD simulations are shown in Figure 9.

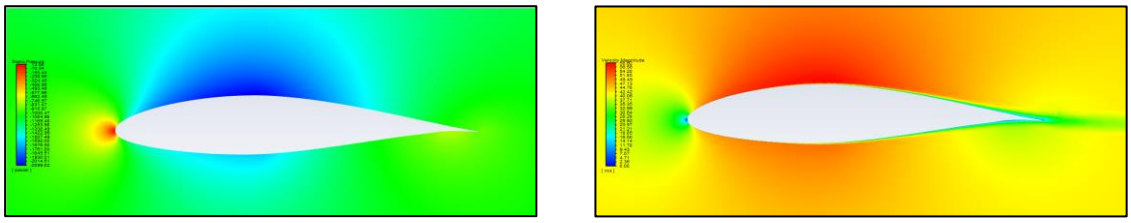

a)

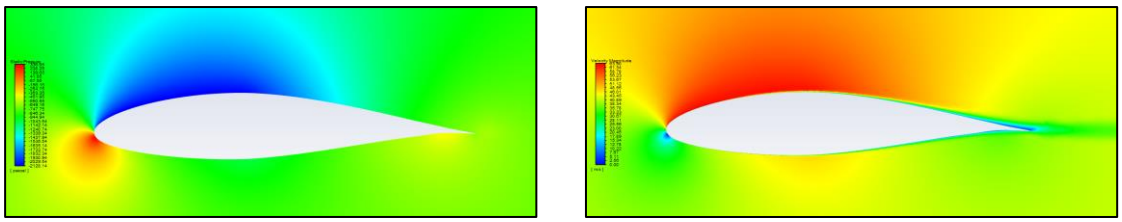

b)

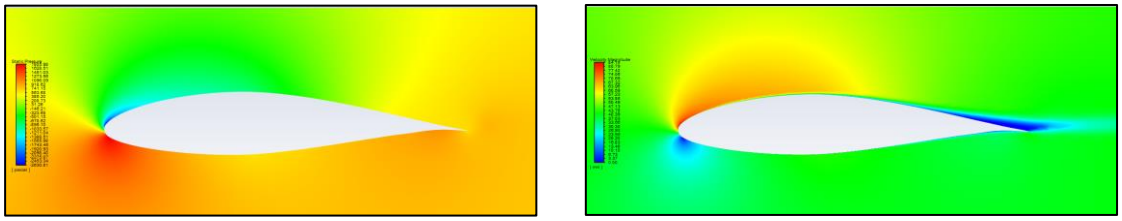

c)

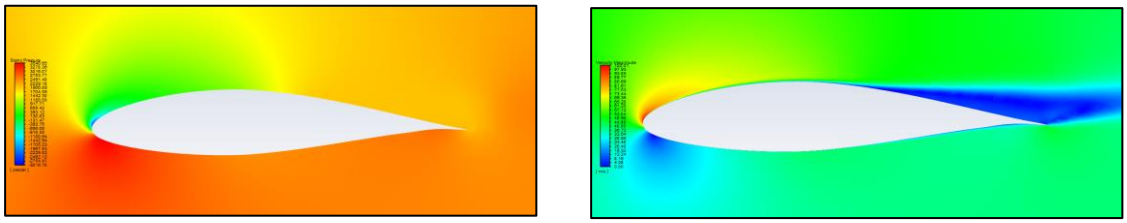

d)

Figure 9: Contours of Static Pressure (left) and Velocity Magnitude (right) for Clean NACA 64-618 a) α=0º b) α=4º c) α=8º d) α=12º

As the pressure on the lower surface of the airfoil is greater than that of the incoming flow, the airfoil is effectively pushed upward normal to the incoming flow, and this means it generates lift. It can also be seen that the pressure gradient increases with an increasing angle of attack. When the pressure gradient is high, the pressure forces overcome the fluid's inertial forces, and the flow starts to separate from the wing surface.

It is observed from Figure 10 that the numerical results are in consistency with experimental results for both lift and drag coefficients. There is a 20 percent error in drag prediction of NACA 64-618. This might be due to the extrapolated value of data at 12º AoA since there was no experimental data at this angle.

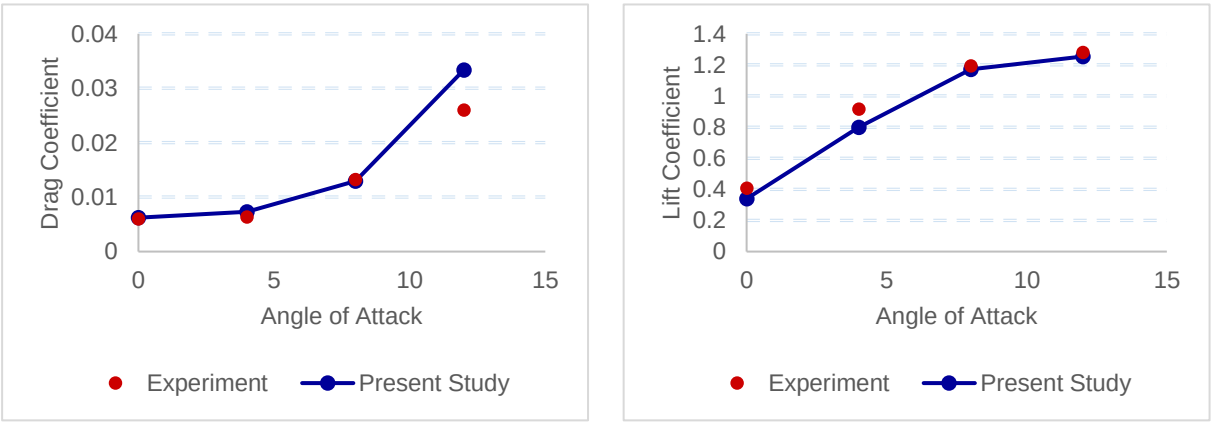

(a) **(b)**

Figure 10: Comparison of Experimental and CFD Results for Clean NACA 64-618 Airfoil a) Drag Coefficient vs. Angle of Attack b) Lift Coefficient vs. Angle of Attack

Iced Airfoil

The contours of pressure and velocity magnitude obtained for α=0º, 4º, 8º and 12º from CFD simulations are shown in Figure 11. The flow accelerates on the upper side of the airfoil and the velocity of flow decreases along the lower side. It can be seen that the pressure is enhanced at the leading edge due to the ice, a no uniform pressure distribution is formed, this directly affects the lift. As a result of ice contamination, the flow separation at the trailing edge is enhanced as the AoA is increased. This has significant impact on decreasing the stall angle.

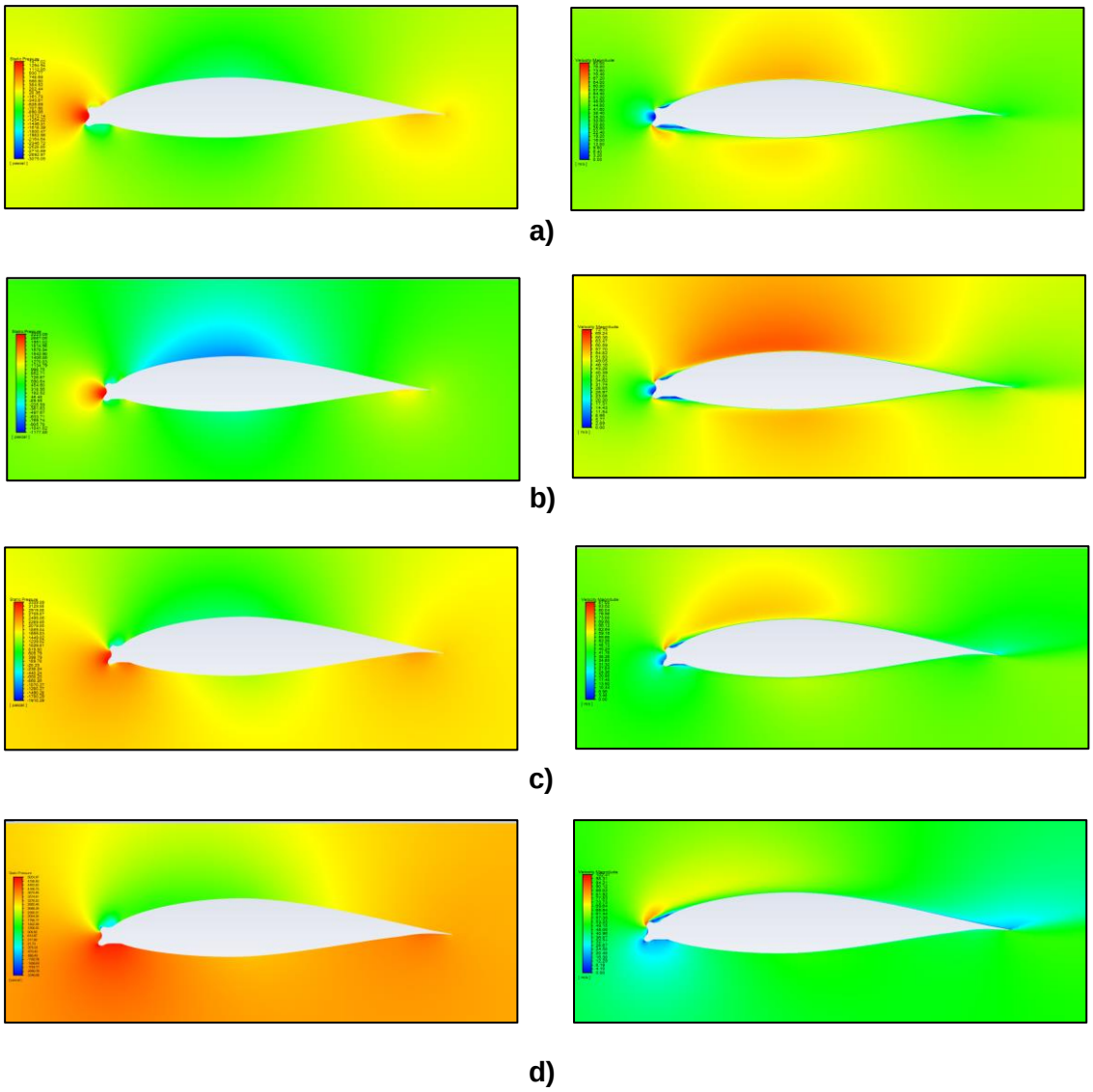

Figure 11: Contours of Static Pressure (left) and Velocity Magnitude (right) for Iced NACA 64-618 a) α=0º b) α=4º c) α=8º d) α=12º

Comparing the clean and iced airfoil velocity contours it can be concluded that the flow separation for the clean airfoil is moderate with a small recirculation zone in the vicinity of the trailing edge while for the iced airfoil the leading-edge flow separation is provoked by the sharp edges of the accreted ice.

The dominant flow feature that determines the aerodynamics of an iced airfoil especially with a horn ice shape is the separation bubble that forms downstream of the horn. This bubble has a global effect on the airfoil pressure distribution iced airfoil aerodynamic. On clean airfoils, the bubble forms when the laminar boundary layer encounters an adverse pressure gradient of sufficient strength to cause separation. On iced airfoils, the boundary layer separates near the top of the horn, due to the pressure gradient produced by the large discontinuity in the surface geometry. In both cases, the separation leads to the formation of a shear layer over the bubble and characteristic flow reversal near the surface [Bragg, Broeren, & Blumenthal, 2005]. Figure 12 shows the upper and lower surface separation streamlines at the leading edge of NACA 64-618 at α=0º, separation bubble is formed downstream the horn ice shape.

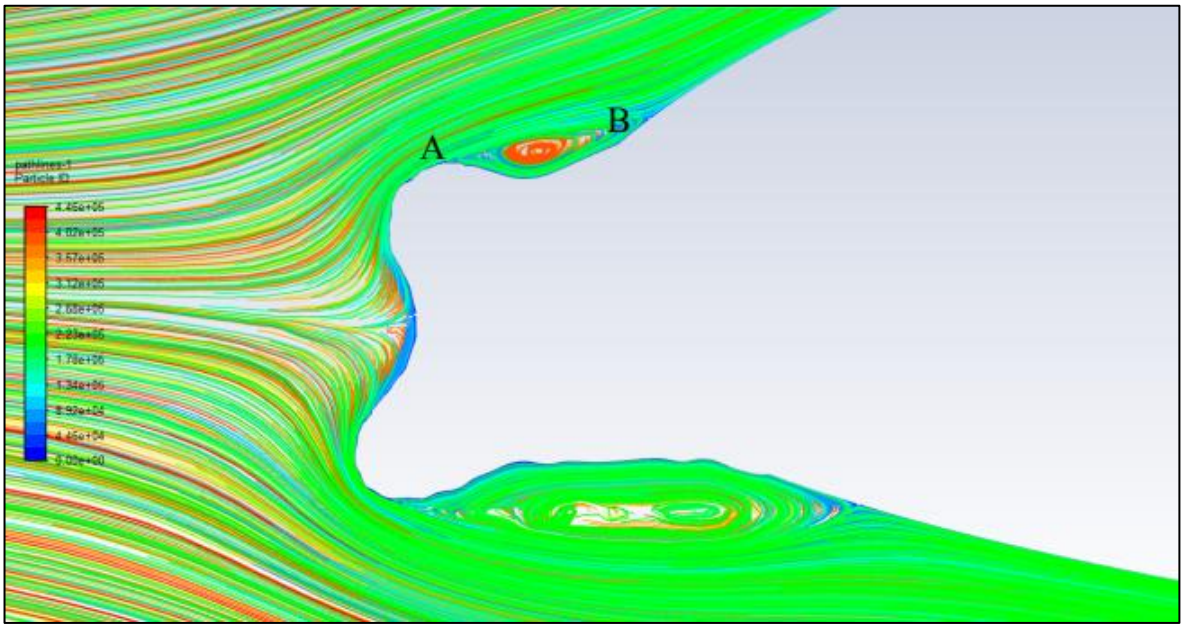

Figure 12: Streamlines at The Leading Edge of Iced NACA 64-618

It is seen at point A that the shear layer transitions to turbulent flow. After transition, the magnitude of the reverse flow increases, and a vortex type flow is seen in the bubble. As the turbulent shear layer entrains high energy external flow, pressure recovery becomes possible, and the bubble reattaches at point B. As the angle of attack increases the upper surface of the separation bubble increases until the bubble fails to entirely reattach.

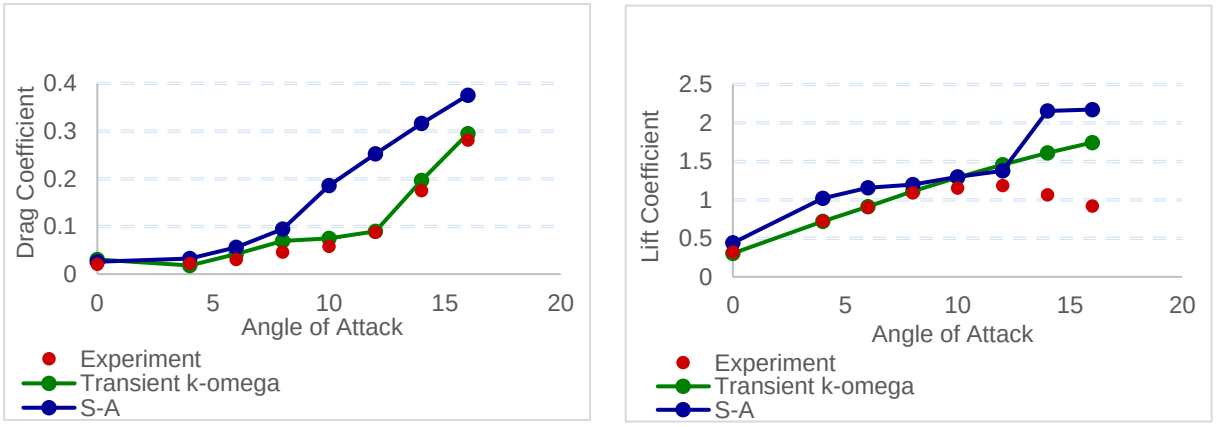

Figure 13: Comparison of Numerical Lift and Drag Coefficients Against Experimental Data for Iced NACA 64-618 Airfoil with Various Turbulence Models.

It is observed from Figure 13 that numerical result shows good agreement at low AoA but over predicts as the angle of attack increases. This error is due to the complex nature of the ice and the challenge of building grids around it. This may be mitigated using a smaller mesh size, especially near the leading edge, so that even smaller feature typical of glaze ice can be modeled. The instability of lift and drag coefficients computed by steady state k-ω SST and S-A models is due to the sharp edges of the ice which causes flow separation, even at low angles of attack. This separation causes unsteady features in the flow which must be analyzed with transient state. The transient results also show a slight deviation from the experimental data. Still, the results computed in Fluent are similar to the experimental value and have general validity. In spite of its deficiencies in predicting some details of the flow, the time dependent k-ω model has proven to be numerically efficient for iced airfoil at low AoA.

In aeroelastic side of the study, aeroelastic analysis and also damping and modal analysis are performed with blade coordinates and boundary conditions. Comparison of blade tune damping eigenvalues with logarithmic decrement is given in Figure 14. It is shown that BEM based aeroelastic models underpredict the stability limit by 5-10% compared to a more comprehensive near wake model. It is also obtained relatively accurate results within this margin based on BEM theory. Related modal results and tune damping frequencies are obtained with blade operational modes and conditions. Comparisons of clean and glazed iced blade modal and damping analysis results are shown in Figures 15 and 16, respectively. It can be seen those obtaining results show there is a misalignment and frequency differences between normal and glazed iced blade model.

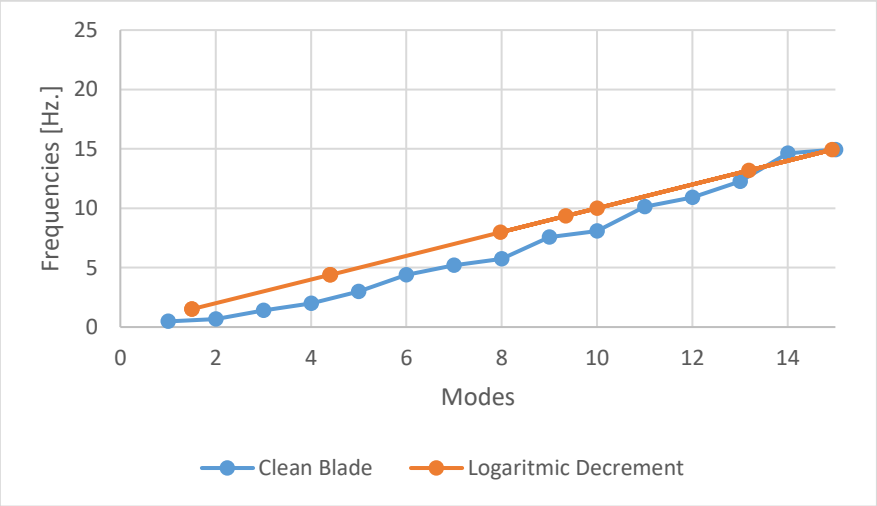

Figure 14: Comparison of Blade Tune Damping Eigenvalues with Logarithmic Decrement

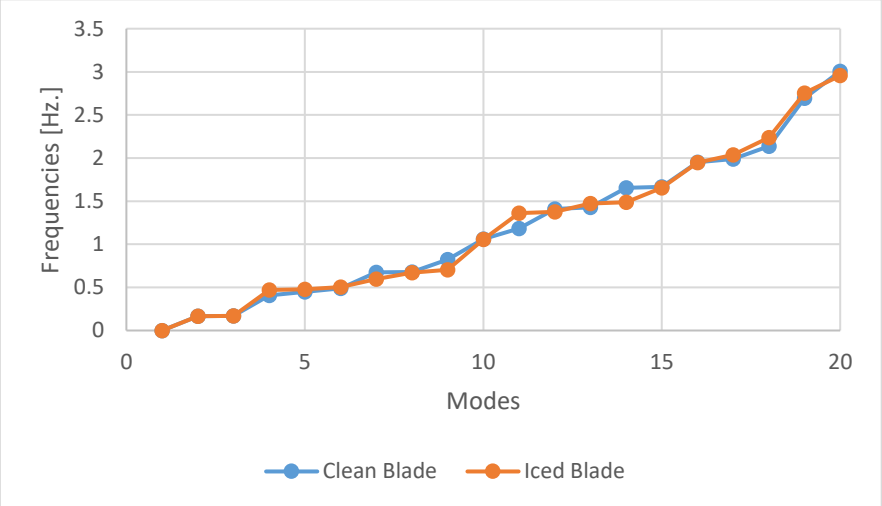

Figure 15: Comparison of clean and Glazed Iced Blade Modal Analysis Results

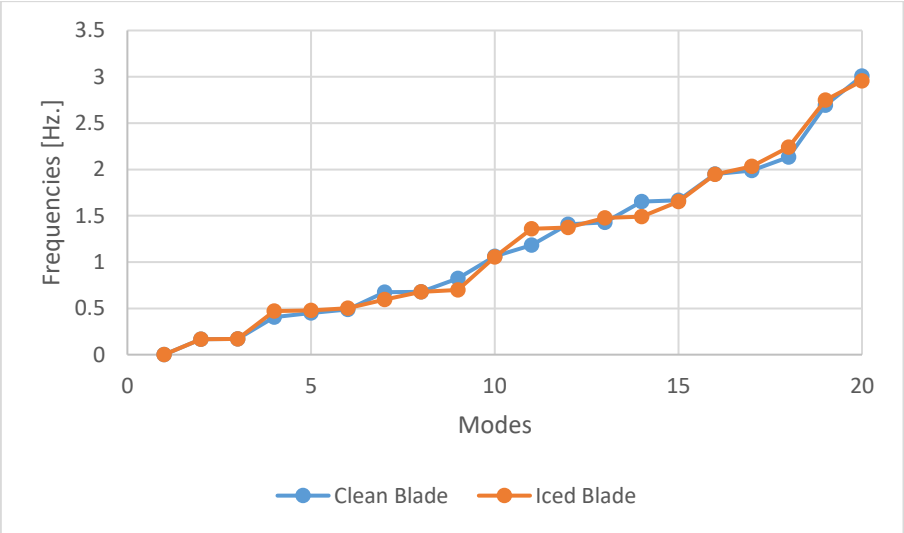

Figure 16: Comparison of clean and Glazed Iced Blade Tune Damping Results

The main post-processing tool is the Matlab function which plots frequencies and logarithmic decrements as function of the wind speed and the mode shapes. Order of modes on a frequency scale should be as expected. First the first flapwise modes, then the first edgewise modes are obtained. Negative damped modes are investigated and issues with resonance are examined by comparing modal frequencies. To compare the blade vibrations and mode shape extraction obtained in the tool, a simple routine has been developed. It requires output of the time series of edgewise and flapwise deflection as well as torsion along the blade. The algorithm fits a cosine function with the variables amplitude a, frequency f and phase φ, moving window of 0.5 seconds of the time series of the flapwise tip deflection, minimizing the error of the cosine fit with the original time series data. The algorithm extracts the mode shape by fitting cosine functions to deflections and rotations at all available radial stations of the blade. The amplitude of 0.1m is chosen because it proved to be a good compromise between extracting the small vibrations at the start of the instability and having large enough amplitudes along the blade to ensure a good performance of the curve fitting algorithm.

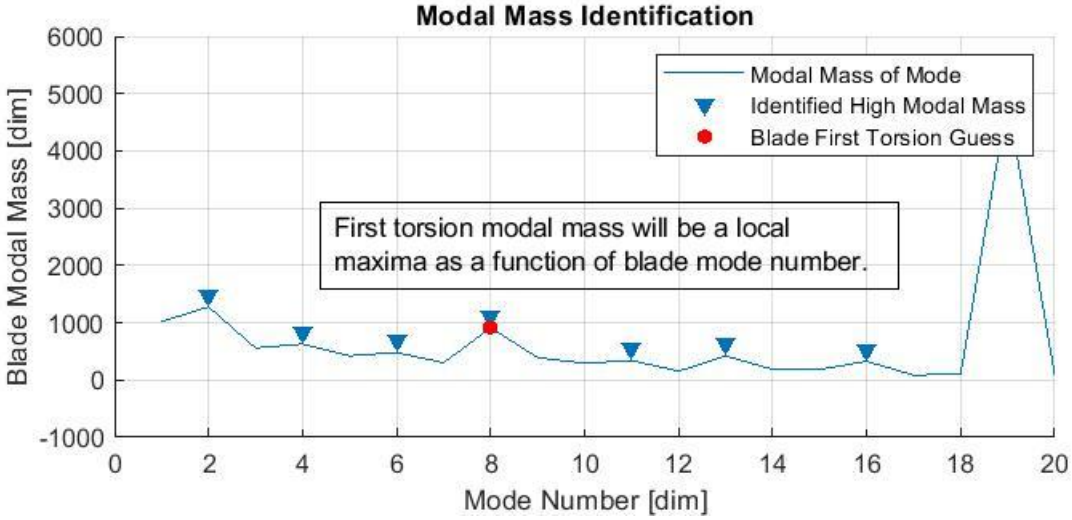

Figure 17: Modal Mass Identifications of Normal and Glazed Iced Blade

In this result, the distributions of both amplitudes and phases of the components of the blade vibration are determined, leading to something similar to mode shapes. The solver is able to capture the structural torsion modes as can be seen in Figure 17. The deflection shapes will

vary with amplitude, so they are not equivalent to mode shapes in linear vibration theory. They can still be used to compare the different instabilities obtained with these different models.

Conclusion

This paper presents a review of the effects of glaze ice on the aerodynamic performance of NACA 64-618. In order to perform the investigations the CFD program ANSYS Fluent was utilized to simulate the flow around the airfoil. Further, the results were compared with the experimental data for validation study of CFD. The clean airfoila was simulated using k-ω SST turbulence model and the transition effects were characterized by intermittency transition model while for the ice case two different models were preferred, the Spalart-Allmaras and the k-ω SST. For clean airfoil case, the numerical results were in good agreement with experimental data but failed in predicting the aerodynamic coefficients for the iced case. This error was due to the complex nature of the ice and the challenge of building grids around it. Also, RANS models perform well in the boundary-layer region but often show poor capabilities in separated regions due to the lack of universality of the turbulence models. The transient results also show a slight deviation from the experimental data. Still, the results computed in Fluent are similar to the experimental value and have general validity.

In aeroelastic side, it can also be seen those obtained tuned damping and modal analysis results of glaze iced and normal blade show glazed iced effects the blade modal frequencies and structural model with the realistic inertial values and turbulence intensity in different wind conditions. It is shown that BEM based aeroelastic models underpredict the stability limit by 5-10% compared to a more comprehensive near wake model. It is also obtained relatively accurate results within this margin. Finally, there is an important interaction between aerodynamic and aeroelastic behavior. In real life, not only the blade but also all other components work under the dynamic characteristics as well so, all the components need to be considered the effect of vibration effect. At least, the blade under the aerodynamic effect which directly feeds back to the angles of attack is demonstrated under the wind conditions. To demonstrate the aeroelastic effect of the blade, a steady structural model with the realistic inertial values and turbulence intensity is modeled considering the effect of the lift and drag.

As we discussed, the accumulation of ice on the blades can affect the performance due to aerodynamic efficiency and on the other hand, because of the increase of ice mass loads, the life of the components can decrease. Therefore, a defined structural model as a comprehensive BEM model to demonstrate exact dynamic behavior according to the related obtained results and the optimum angle of attack values will be determined to find the optimum distribution in each wind speed on the system.

It is shown that BEM based aeroelastic models under predict the stability limit by 5-10% compared to a more comprehensive near wake model. It is also obtained relatively accurate results within this margin based on BEM theory. Related modal results and tune damping frequencies are obtained with blade operational modes and conditions. It can be seen that a misalignment and frequency differences are found for the mode shapes and maximum deflection of normal and glaze iced blade under different wind speed conditions. It is revealed that glazed iced blade should investigate aerodynamic efficiency with aeroelastic effect under different wind conditions.

References

Addy, H. E. (2000). *Ice Accretions and Icing Effects for Modern Airfoils*. (S.l.) : (s.n.).
Alzaili, J. S. L. (2012). Semi-Empirical Approach to Characterize Thin Water Film Behaviour in Relation to Droplet Splashing in Modelling Aircraft Icing, *66*(July), 37-39.
Anderson, D. N. (2004). Manual of Scaling Methods. *NASA Glenn Research Center*, (March), 80.
Bragg, M. B., Broeren, A. P., & Blumenthal, L. A. (2005). Iced-airfoil aerodynamics. *Progress in Aerospace Sciences*, *41*(5), 323-362. https://doi.org/10.1016/j.paerosci.2005.07.001
Brown, C. M. (2013). Computational Modelling of Rotor Blade Performance Degradation Due to Ice Accretion, (December).
Etemaddar, M., Hansen, M. O. L., & Moan, T. (2013). Wind Turbine Aerodynamic Response Under Atmospheric Icing Conditions. *Wind Energy*, (November 2012), 1-20. https://doi.org/10.1002/we
Hann, R. (2018). UAV icing: Comparison of LEWICE and FENSAP-ICE for ice accretion and performance degradation. *2018 Atmospheric and Space Environments Conference*, 1-8. https://doi.org/10.2514/6.2018-2861
Homola, M. C., Virk, M. S., Wallenius, T., Nicklasson, P. J., & Sundsbø, P. A. (2010). Effect of Atmospheric Temperature and Droplet Size Variation on Ice Accretion of Wind Turbine Blades. *Journal of Wind Engineering and Industrial Aerodynamics*, *98*(12), 724-729. https://doi.org/10.1016/j.jweia.2010.06.007
Ruff, G. A. (1985). Analysis and Verification of the Icing Scaling Equations. *Aedc-Tr-85-30*, *1*.

Glauert, Airplane propellers. In Durand, WF (ed.) Aerodynamic Theory, 4th edition, (1935) 169–360. Springer.
Craig, R. and Bampton, M. (1968). Coupling of Substructures for Dynamic Analysis. AIAA Journal, 6(7).
Hansen, M.H., Aeroelastic instability problems for wind turbines. Wind Energy, 2007.

Manwell J. F., McGoan J. G. and Rogers A. L., Wind Energy Explained: Theory, Design and Application. Wiley & Sons, Ltd., 2002.
Den Hartog, J.P., “Advanced strength of materials”, McGraw Hill, 1952
G. R. Pirrung, H. A. Madsen and T. Kim, The influence of trailed vorticity on flutter speed estimations.
IEC 61400-1 third edition 2005-08 Wind turbines – Part 1: Design requirements, International Electrotechnical Commission, IEC, 2005.
Abbott, I.H. and Von Doenhoff, A.E. (1959) Theory of Wing Sections: Including a Summary of Airfoil Data. Dover Publications, Mineola.